Mon. Not. R. Astron. Soc. **000**, 000–000 (0000) Printed 2 February 2008 (MN LATEX style file v2.2)

Galactic Centre stellar winds and Sgr A* accretion

Jorge Cuadra‡, Sergei Nayakshin§, Volker Springel & Tiziana Di Matteo†

Max-Planck-Institut für Astrophysik, Karl-Schwarzschild-Straße 1, 85741 Garching bei München, Germany

arXiv:astro-ph/0505382v2 9 Nov 2005

2 February 2008

ABSTRACT

We present a detailed discussion of our new 3D numerical models for the accretion of stellar winds on to Sgr A*. In our most sophisticated models, we put stellar wind sources on realistic orbits around Sgr A*, we include recently discovered 'slow' winds ($v_{\rm w} \sim 300$ km s^{-1}), and we account for optically thin radiative cooling. We test our approach by first modelling only one phase 'fast' stellar winds ($v_{\rm w} \sim 1000$ km s^{-1}). For stellar wind sources fixed in space, the accretion rate is of the order of $\dot{M} \simeq 10^{-5}\,{\rm M}_\odot$ yr^{-1}, fluctuates by $\lesssim 10\%$, and is in a good agreement with previous models. In contrast, $\dot{M}$ decreases by an order of magnitude for wind sources following circular orbits, and fluctuates by $\sim 50\%$. Then we allow a fraction of stars to produce slow winds. Much of these winds cool radiatively after being shocked, forming cold clumps and filaments immersed into the X-ray emitting gas. We investigate two orbital configurations for the stars in this scenario, an isotropic distribution and two rotating discs with perpendicular orientation. The morphology of cold gas is quite sensitive to the orbital distribution of the stars. In both cases, however, most of the accreted gas is hot, producing a quasi steady 'floor' in the accretion rate, of the order of $\sim 3\times10^{-6}\,{\rm M}_\odot$ yr^{-1}, consistent with the values deduced from *Chandra* observations. The cold gas accretes in intermittent, short but powerful accretion episodes which may give rise to large amplitude variability in the luminosity of Sgr A* on time scales of tens to hundreds of years. The circularisation radii for the flows are about 10^3 and 10^4 Schwarzschild radii, for the one and two-phase wind simulations, respectively, never forming the quasi-spherical accretion flows suggested in some previous work. Our work suggests that, averaged over time scales of hundreds to thousands of years, the radiative and mechanical luminosity of Sgr A* may be substantially higher than it is in its current state. Further improvements of the wind accretion modelling of Sgr A* will rely on improved observational constraints for the wind velocities, mass loss rates and stellar orbits.

Key words: Galaxy: centre – accretion: accretion discs – galaxies: active – methods: numerical – stars: winds, outflows

1 INTRODUCTION

Sgr A* is believed to be a super-massive black hole (SMBH) of mass $M_{\rm BH} \simeq 3.5\times10^6\,{\rm M}_\odot$ in the very centre of our Galaxy (e.g., Reid et al. 1999; Schödel et al. 2002; Ghez et al. 2003). Winds from young massive stars with velocity $v_{\rm w}$ around 1000 km s^{-1} are known to fill the inner parsec (e.g., Hall et al. 1982) with hot plasma. The total mass loss rate from these stars is $\sim 10^{-3}\,{\rm M}_\odot$ yr^{-1} (e.g., Genzel et al. 1994; Najarro et al. 1997), and a fraction of this gas should be accreting on to the SMBH (e.g., Melia 1992). The observed luminosity is however many orders of magnitude smaller than what is predicted from the classical Bondi-Hoyle theory (Bondi 1952). There are two possible explanations for this discrepancy: either a much smaller amount of gas actually accretes on to the SMBH or accretion proceeds in a low-radiative efficiency mode. The current consensus appears to be that both of these factors are important for reducing Sgr A*'s luminosity (Narayan 2002). From theoretical arguments, it is unlikely that the accretion flow is exactly spherical, and instead it is plausible that a rotating flow forms in which the resulting viscous or convective heating unbinds much of the gas, severely reducing the accretion rate (Blandford & Begelman 1999; Quataert & Gruzinov

‡ E-mail: jcuadra@mpa-garching.mpg.de
§ Current address: Department of Physics & Astronomy, University of Leicester, Leicester LE1 7RH, UK
† Current address: Department of Physics, Carnegie Mellon University, Pittsburgh, PA 15213, USA

2000). It is also likely that electrons are not as hot as the ions, thus resulting in a greatly diminished radiative efficiency of the flow (Narayan & Yi 1994).

Observations of Sgr A* in the radio and in the X-ray bands constrain the accretion rate at tens of Schwarzschild radii distance from the SMBH to values of the order of $\dot{M}_{\rm in} \sim {\rm few}\times 10^{-7}\,{\rm M}_\odot\ {\rm year}^{-1}$ (Bower et al. 2003; Nayakshin 2005). This is significantly smaller than the $\sim 3\times 10^{-6}\,{\rm M}_\odot\ {\rm year}^{-1}$ accretion rate estimated based on *Chandra* observations at $\sim 10^5$ Schwarzschild radii (Baganoff et al. 2003), confirming that gas outflows are important. For the sake of closer testing accretion flow theories, it is important to establish the exact amount of gas captured by Sgr A* to compare to $\dot{M}_{\rm in}$. Note that this exercise can be done only for Sgr A* at present, since all other AGN are much farther away, and hence Sgr A* is a unique test object in this regard.

The first three dimensional numerical simulations of Sgr A* wind accretion were performed by Ruffert & Melia (1994), who studied feeding the black hole from a uniform large scale gas flow. This work was extended by Coker & Melia (1997), who used discrete gas sources, ten mass-loosing stars semi-randomly positioned a few arc-seconds away from Sgr A*, to model the wind emission. Due to numerical difficulties inherent to fixed grid codes, the orbital motions of the stars could not be followed, and thus they were fixed in space. The authors argued that such an approach is valid since the wind velocities, as best known at the time, are larger than the circular Keplerian motions of the stars in these locations. Moreover, if the stellar orbits are isotropically distributed, and all stars are identical, then the net angular momentum is nearly zero. More recently, Rockefeller et al. (2004) used a particle-based code, making also use of more detailed information on stellar coordinates and wind properties. However, the stars once again were kept at fixed locations.

Recent near-IR data of the nuclear star cluster in Sgr A* show that the stellar wind sources are located in two ring- or disc-like distributions that are roughly perpendicular to each other (Paumard et al. 2001; Genzel et al. 2003), implying that shocked gas has a non-zero net angular momentum. This is likely to be important for understanding the structure of the accretion flow. In addition, integral field spectroscopy of the central parsec implies stellar wind velocities of only ~ 200 km s^{-1} (Paumard et al. 2001); much less than the values of ~ 600 km s^{-1} previously estimated. These new data imply that stellar orbital motions are more important than previously thought. Moreover, these slow winds, when shocked, are heated to around 10^6 K as opposed to the temperature of $1-2\times 10^7$ K for the hotter ~ 1000 km s^{-1} winds. This former slow phase of Sgr A* stellar winds is therefore susceptible to radiative cooling (Cuadra et al. 2005) and thus it is expected to form a *cold* gas flow on to Sgr A* in addition to the usually studied hot non-radiative phase.

Motivated by the new observations and the above ideas, we performed numerical simulations of wind accretion on to Sgr A* including optically thin radiative cooling and allowing the wind-producing stars to be on circular Keplerian orbits. Some preliminary results of our study have already been presented by Cuadra et al. (2005). Here we report on specific tests of our new methodology and provide further details on our results. While this study sheds new light on physics of accretion of stellar winds on to Sgr A*, it is clear that improved observational determinations of stellar mass loss rates, wind velocities, stellar orbits, and also of orbits and distribution of the cooler gas phase filling in the inner parsec will be the key for further improving our understanding of the Galactic centre region.

The paper is structured as following. We describe our numerical method in Section 2, and give results of simulations with single, fast wind velocity in Section 3, including a comparison with analytic models. In Section 4, we then describe our results for simulations with fast and slow ('two-phase') winds, followed in Section 5 by an analysis of fiducial *Chandra* observations of our simulated systems. We give a detailed discussion of our results in Section 6, and conclude in Section 7.

2 THE NUMERICAL METHOD

We use the SPH/N-body code GADGET-2 (Springel et al. 2001; Springel 2005) to simulate the dynamics of stars and gas in the (Newtonian) gravitational field of Sgr A*. This code solves for the gas hydrodynamics via the smoothed particle hydrodynamics (SPH) formalism. The hydrodynamic treatment of the gas includes adiabatic processes, artificial viscosity to resolve shocks, and optically thin radiative cooling with the cooling function $\Lambda \approx 6.0\times 10^{-23}(T/10^7\,{\rm K})^{-0.7}\,{\rm erg\ s^{-1}\,cm^{-3}}$ (Sutherland & Dopita 1993).

The SMBH is modelled here as a heavy collisionless particle with gravitational smoothing length of $0.01''$. In addition it acts as a sink particle: gas passing within the inner radius $R_{\rm in}$ disappears, giving up its mass and momentum to the black hole (Springel et al. 2004; Di Matteo et al. 2005). The inner radius in our model is a free parameter, but for most tests we pick it to be $\lesssim 0.1''$, much smaller than the capture, or Bondi radius, $R_{\rm capt} = GM_{\rm BH}/(c_{\rm s}^2+v_{\rm w}^2)$, where $c_{\rm s}$ is the gas sound speed and G the gravitational constant. For the case of Sgr A*, X-ray observations yield $R_{\rm capt}\sim 1''$ (Baganoff et al. 2003).

At least 99% of the 'wind' (gas) particles escape from the region of interest, the inner $\sim 10''$, into the Galaxy. Following these particles in a region which we do not model properly here becomes prohibitively expensive, and is of limited interest for the problem at hand. Therefore we eliminate SPH particles that reach an 'outer radius' $R_{\rm out}$. We found that setting $R_{\rm out}$ larger than the distance from the outermost wind source to the SMBH is appropriate for our purposes.

Stellar winds are modelled via 'emission' of new gas (SPH) particles by the star particles from which these winds emanate. Ejection of particles is done typically in bursts of about 30 particles per star and occurs in time intervals of 0.2–1 yrs. For each group of new SPH particles a random isotropic velocity distribution is generated. For tests with moving stars, the full initial particle velocity is the sum of its random isotropic part (in magnitude equal to the specified wind velocity $v_{\rm w}$) and the stellar 3-D velocity. The new particles are given initial temperature of 10^4 K, which is also the minimum temperature the gas is allowed to have in the simulations. As we are not interested in resolving the wind structure close to stellar surface, we also give the particles small spatial 'kicks' along their velocities. Baring

this, we would have to resolve extremely small scale structures around stellar surfaces which is not feasible numerically. The rest of the SPH properties (pressure, density, entropy, etc.) are then calculated and followed self-consistently by the code.

3 MODELS WITH FAST WINDS

A realistic modelling of Sgr A* wind accretion requires several steps of varying complexity and importance for final results. In this section we shall start by considering the 'single-phase' case when the properties of all the wind sources are identical. We are interested in the dependence of the results on the number of sources, their distribution and their orbital motion, as well as on the choice of our free parameter $R_{\rm in}$.

3.1 Fixed stars

A very useful test for our numerical methods is the comparison with analytical results. Quataert (2004) presented an analytical 1-D (spherical) model for the hot gas in the Galactic Centre. He distributed wind sources in a spherical shell between radii 2–10″ with stellar number density $n_*(r) \propto r^{-\eta}$, where η is a free parameter varying between 0 and 3. The winds are further assumed to shock and be thermalized locally. Essentially, this model is a spherical wind/Bondi accretion model with distributed wind sources, and as such it presents a very convenient test bed for our numerical methods.

In the context of our numerical models, the 'on the spot' thermalization of winds is identical to having an infinite number of wind sources, since then the mean distance between them is zero and winds are thermalized immediately. In practice, we ran simulations with 200 stars isotropically and randomly distributed in the same range of radii, with a density profile given by the $\eta = 2$ power-law. Our first objective is to test the sensitivity of the results to different values for the inner radius, $R_{\rm in} = 0.1,\ 0.4,\ 1''$. The outer boundary is set at $R_{\rm out} = 15''$ for these tests. We ran tests with larger values for $R_{\rm out}$ and found that the results depend little on this value as long as it includes all the wind sources. The total mass loss rate of stars is set to $\dot{M}_{\rm w} = 10^{-3}\,{\rm M}_\odot\,{\rm yr}^{-1}$, and the wind velocity is $v_{\rm w} = 1000\,{\rm km\,s}^{-1}$.

We ran these simulations until time $t \sim 2100\,{\rm yr}$, at which the system is in a quasi-steady state. The number of SPH particles in the steady state is $\simeq 10^6$. To improve statistics, the radial profiles of quantities of interest are averaged over the last 10 snapshots covering the time interval $t \approx 1800 - 2100\,{\rm yr}$. The resulting density profiles are shown in Fig. 1, together with the result from Quataert (2004) (the model with $\eta = 2$)[1]. Except for the flattening at radii approaching $R_{\rm in}$, where the SPH particle density is underestimated due to our 'capture all' boundary condition there, the curves are in good agreement.

Figure 2 shows the average radial velocity as a function of radius for the same runs. The radial velocity curves differ

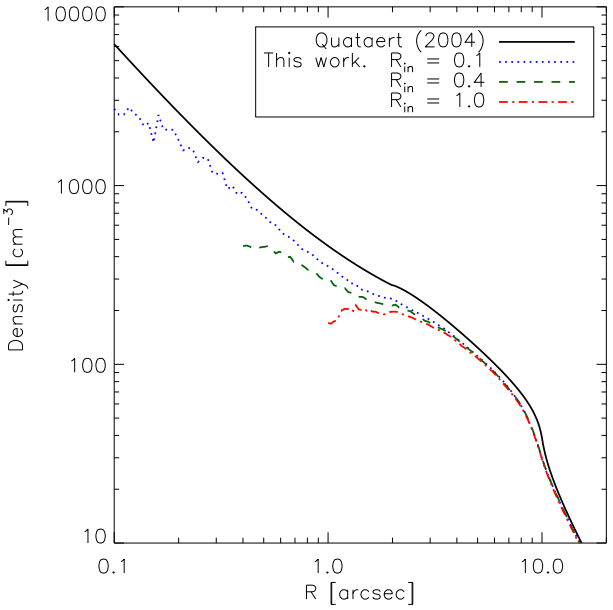

Figure 1. Radial density profiles of the gas in simulations with 200 fixed stars, distributed isotropically. The black solid curve shows the model of Quataert (2004). Note that our curves (coloured lines) reproduce his solution rather well down to about twice $R_{\rm in}$. The values of $R_{\rm in}$ for the different simulations are given in the inset.

more from the Quataert (2004) curve (solid line) than the density curves. Our vacuum inner boundary condition forces the gas next to $R_{\rm in}$ to inflow with velocity approaching the gas sound speed. Clearly, when $R_{\rm in}$ is large, this inflow velocity is larger than that of the Bondi (1952) solution at that point. Hence simulations with large values of $R_{\rm in}$ will over-estimate the accretion rate on to the SMBH (we discuss this point in more detail below). If instead $R_{\rm in}$ is a factor of at least several smaller than $R_{\rm capt}$, we expect to closely match Quataert (2004)'s results because by that point the inflow speed of the Bondi (1952) solution is approaching the local sound speed. This should be achieved in the simulation with the smallest inner boundary ($R_{\rm in} = 0.1''$). While we do obtain very similar gas densities (Fig. 1), the inflow velocity is significantly lower in our simulation than in the analytical solution. We find that, even with 200 sources, the accretion flow is still strongly anisotropic in the sub-arcsecond region. Indeed, most of the wind is unbound, with as little as $\sim 1\%$ accreting on to Sgr A*. Thus, out of 200 sources, only the ~ 10 innermost stars are important for accretion. This can be seen through the gas velocity profile: the radial velocity changes its sign just above the inner radius of the wind-source region. In addition, as will become clear later, the incomplete thermalization of the winds does lead to some excess energy in the wind, and thus *not all* of the gas within the nominally defined accretion radius is actually bound. Some of the gas at $R < R_{\rm capt}$ may therefore have a positive radial velocity.

Effects that are due to the finite number of stars should also manifest themselves in cooler temperature profiles at large radii compared to the Quataert (2004) results. There is a finite distance the winds will travel before they will

[1] We multiplied Quataert (2004)'s density by a factor 2, since his models were actually computed for $\dot{M}_{\rm w} = 5 \times 10^{-4}\,{\rm M}_\odot\,{\rm yr}^{-1}$ (Quataert, priv. comm.).

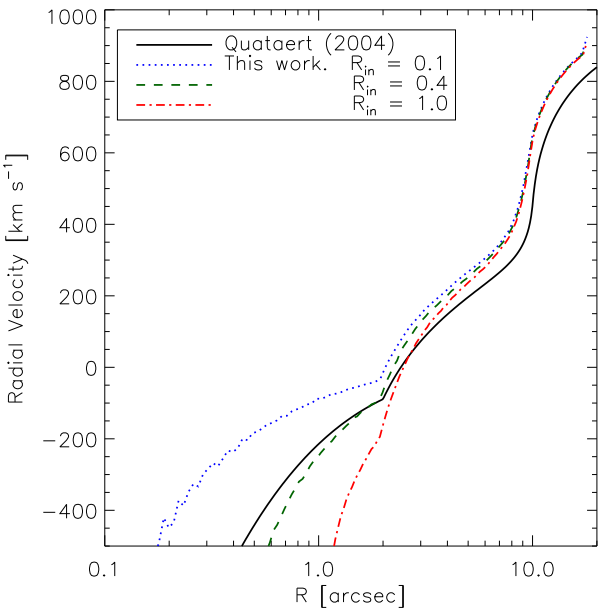

Figure 2. Radial velocity profiles of the gas in the calculations with 200 fixed stars distributed isotropically. Note that for larger capture radius the gas inflows faster. Because of the finite number of sources, the outflow velocity of our simulations is slightly larger than that in Quataert (2004).

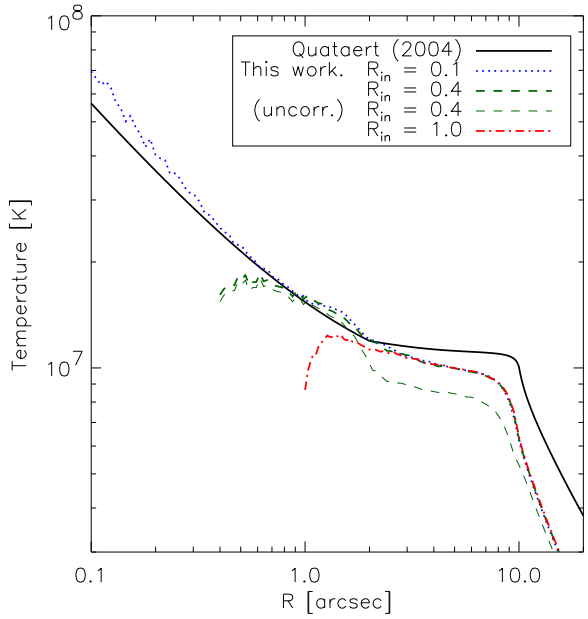

Figure 3. The '1-d' temperature profiles of gas for the simulation with 200 fixed, isotropically distributed stars. The definition of $T_{\rm 1d}$ includes gas bulk motions that would be absent in the case of exact spherical symmetry; $T_{\rm 1d}$ is to be compared with the semi-analytical curve of (Quataert 2004, solid). The 'raw' gas temperature, uncorrected for the bulk gas motions, is given for the case of $R_{\rm in} = 1''$ (lower red curve).

experience a shock that will heat the gas up to the expected temperature. Therefore, for comparison purposes, we also defined an 'effective 1-dimensional' temperature $T_{\rm 1d} = T + (m_{\rm p} v_{\rm nr}^2)/(10 k_{\rm B})$, where $m_{\rm p}$ is the proton mass and $k_{\rm B}$ is the Boltzmann constant. The quantity $\boldsymbol{v}_{\rm nr} = \boldsymbol{v} - \langle |\boldsymbol{v}\cdot\hat{\boldsymbol{r}}| \rangle \hat{\boldsymbol{r}}$ is the local gas velocity minus the mean radial velocity at the given radius. In a strictly spherically symmetric model (with an infinite number of stars) the non-radial velocity $\boldsymbol{v}_{\rm nr}$ would of course be zero, with the corresponding energy converted into thermal energy of the gas. Therefore $T_{\rm 1d}$ is the quantity to compare with the temperature derived by Quataert (2004). Figure 3 shows radially averaged $T_{\rm 1d}$ profiles, and, for the case $R_{\rm in} = 0.4''$, we also show the actual uncorrected gas temperature T (lower green curve), also averaged in radial shells. Note that the difference between $T_{\rm 1d}$ and T is only significant at radii greater than $1''$ because inside this radius the gas is relatively well mixed, i.e. shocked. On the contrary, the average gas temperature in the outflow region (close to our outer boundary condition) is significantly smaller than the spherically-symmetric limit. The reason for this is that some of the wind from the outermost stars is actually never shocked as it escapes from the computational domain. The same reason is also responsible for the differences in the radial velocity curves (Fig. 2): all of our solutions outflow slightly faster at $R \lesssim R_{\rm out}$ than do the winds of Quataert (2004).

The accretion rate, $\dot{M}_{\rm BH}$, in our simulations is defined as the total mass entering the sphere of radius $R_{\rm in}$ per unit time. We find that the accretion rate increases initially while winds fill in the available space, but after less than 1,000 years $\dot{M}_{\rm BH}$ reaches a steady state value. The final value will of course depend on the choice of $R_{\rm in}$. For the simulations described above, we get accretion rates $\dot{M}_{\rm BH} \approx 1.5$, 3.5 and $7 \times 10^{-5}\,{\rm M}_\odot\ {\rm yr}^{-1}$, for $R_{\rm in} = 0.1, 0.4,$ and $1''$ respectively. The increase of $\dot{M}_{\rm BH}$ with $R_{\rm in}$ implies that a significant fraction of the gas that is 'accreted' in the simulations with large $R_{\rm in}$ would not have done so had we been able to resolve the smaller scale flow. As far as the exact accretion rate values are concerned, smaller $R_{\rm in}$ is better, but, since a smaller $R_{\rm in}$ requires shorter integration steps, one has to make a pragmatic compromise and choose a value of $R_{\rm in}$ that allows simulations to be run in a reasonable time.

The accretion rates that we obtain are comparable with the Quataert (2004) result for $\eta = 2$, $4.5 \times 10^{-5}\,{\rm M}_\odot\ {\rm yr}^{-1}$. However, the most reliable of the tests, with $R_{\rm in} = 0.1''$, shows an accretion rate a factor of 3 lower than the semi-analytical result. We interpret this as another manifestation of the incomplete spherical symmetry due to the finite number of stars in our simulations. We found that even at radii as small as $0.3''$ there are large deviations from the mean in the gas velocity in the same radial shell. In addition, a fraction of the gas has significant specific angular momentum. To test these points further, we ran an additional simulation with $R_{\rm in} = 0.1''$, but with 40 wind sources, which is more realistic as far as Sgr A* wind accretion is concerned but should enhance the discreteness effects when compared with Quataert (2004). The results we obtain are in general similar, but the effects produced by the finite number of sources are indeed enhanced. For example, the density in the inner region is $\sim 50\%$ lower than in the simulation with 200 stars, producing a corresponding lower accretion rate (see green curves in Figs. 5 and 6).

We find that our derived accretion rate values are about

one order of magnitude lower than those of Coker & Melia (1997). The differences are however due to a different physical setup rather than numerics. Coker & Melia (1997) used $v_{\rm w} = 700$ km s^{-1}, whereas we used $v_{\rm w} = 1000$ km s^{-1} here. This difference in wind velocity alone accounts for a factor of ≈ 3 difference in $\dot{M}_{\rm BH}$. Furthermore, their total mass loss rate from the young stars is higher than ours by a factor of 3. If we take into account these differences, our simulation with the smallest capture radius and 40 fixed stars appears to be consistent with the results of Coker & Melia (1997). Finally, the work of Rockefeller et al. (2004) did not directly focus on the accretion on to Sgr A*. They were mainly interested in the dynamics of gas on parsec-scales. The accretion rate they quote is likely to be over-estimated because of the large value of $R_{\rm in} \approx 2''$ they use.

3.2 Stars in orbits around Sgr A*

The next step towards a more realistic model is to allow the stars to follow orbits in Sgr A*'s gravitational potential. We do this in two idealised configurations: a spherically symmetric and a disc-like system (for the latter, the stellar disc is somewhat thick, with $H/R \sim 0.2$, as seems to be the case observationally). In both cases, we put 40 stars in circular orbits around the SMBH. We use the same stellar density profile as in Section 3.1, $n_*(r) \propto r^{-2}$, and boundary conditions $R_{\rm in} = 0.1''$, $R_{\rm out} = 18''$.

The significant difference with respect to the simulations discussed in Section 3.1 is that now the gas particles have a significant net angular momentum. To quantify this we create radial profiles of the average angular momentum, defined as the modulus of the average angular momentum vector in a shell, $l(r) = |\langle \boldsymbol{r} \times \boldsymbol{v} \rangle|$. Since we measure distances in arc-seconds and velocities in units of circular Keplerian velocity at that distance, a circular orbit at $r = 1''$ has $l(1'') = 1$ in these units. Note that $l(r)$ should vanish for an isotropic orbital distribution of wind sources, even if each individual gas particle has a high angular momentum. Figure 4 shows the $l(r)$ profiles for the simulations described in this section, and for the one with 40 fixed stars from Section 3.1.

When the stars are confined to a disc (red curve), the gas has on average roughly the local Keplerian angular momentum at the 'wind source' region, simply because the stars are on Keplerian circular orbits with the same angular momenta direction. If the orbits are randomly oriented (blue), the angular momenta of the gas should cancel out owing to the symmetry. However, the cancellation is incomplete due to the finite number of sources. Finally, in the case where the stars are fixed (green), the angular momentum is negligible, as it should.

Comparing the angular momentum in the three simulations in the sub-arcsecond region, we see that all simulations yield similar results. In all the cases the gas in this region is rotating significantly slower than the local Keplerian rotation, indicating that centrifugal support is not important for the gas. This is somewhat surprising given the vastly different angular momentum curves at larger radii and is not a result of viscous transport processes, because a physical viscosity was not included in the simulations[2]. This result

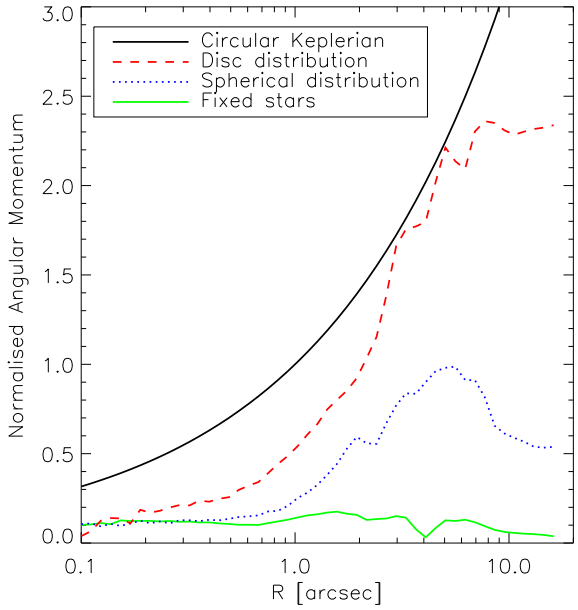

Figure 4. Angular momentum averaged on radial shells, $l(r)$, in the simulations with 40 stars in circular orbits (red and blue lines) and in fixed positions (green). For comparison we also show the value of the angular momentum of a circular orbit (black).

rather seems to indicate that only the gas with originally low enough angular momentum makes it into the innermost region and is subsequently accreted, as already discussed by Coker & Melia (1997). The fraction of the stellar wind with low angular momentum however varies greatly between the simulations, which in turn explains the different accretion rates.

Note that, once again due to the finite number of stellar sources, there is a distribution in the values of the gas angular momentum for any given radius. Some of the gas at $R \sim 0.5''$, for example, has a roughly Keplerian angular momentum which prevents it from accreting. This gives rise to shallower density profiles, as seen in Fig. 5, and is particularly important in the disc simulation (red curve), where the density is 2–3 times lower at $1''$ than in the case with fixed stars. Note that in this case, the density value at $1''$ is in better agreement with densities implied by *Chandra* observations (Baganoff et al. 2003). Correspondingly, the mass supply to the central black hole also decreases: we find that in the simulation with stars located in a disc, the average accretion rate is only $\sim 2 \times 10^{-6}\,{\rm M}_\odot$ yr^{-1}, about 5 times lower than the value found with fixed stars.

In addition to these effects, stellar motions yield a significant variability in the accretion rate. Figure 6 shows the accretion rate as a function of time for the same three simulations. In all the simulations, the accretion rate increases initially, as the stellar winds fill up the space. In the run with fixed stars, the accretion rate is practically constant after this initial increase. In contrast, when stars are allowed to follow orbits, the geometry of the stellar system

[2] Note that the fact that the gas is significantly sub-Keplerian in the region justifies our neglect of angular momentum transport by viscosity.

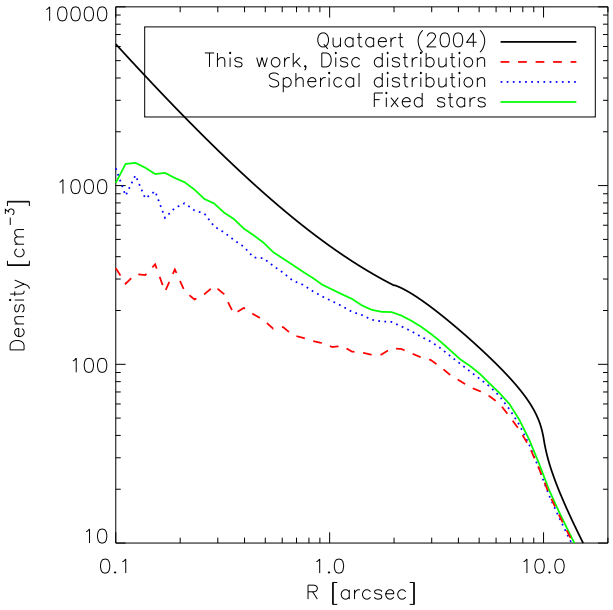

Figure 5. Density profiles of the gas in the calculations with 40 stars for different orbital configurations. The presence of significant angular momentum prevents the gas from inflowing, resulting in a lower density in the inner part.

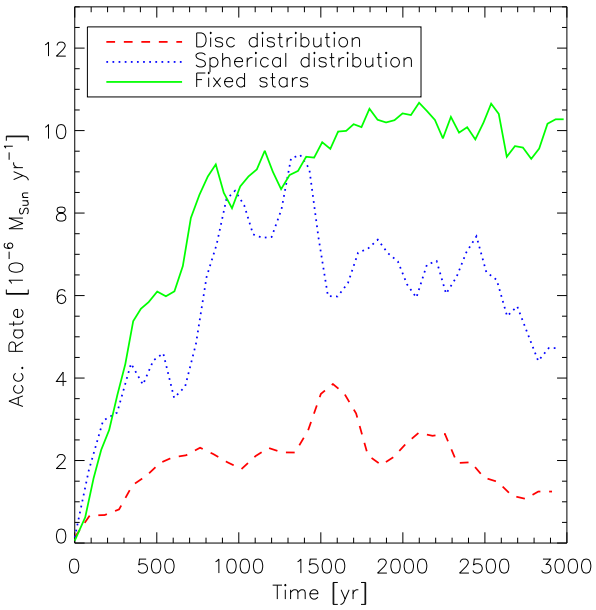

Figure 6. Accretion rate as a function of time in the simulations with 40 stars for different orbital configurations. The rotation of the stars produces a lower but variable accretion rate.

changes with time (both in the isotropic and disk-like configurations), and so does the fraction of gas that can flow to the inner region. We should emphasise that this factor of $\sim 30-70\%$ variability occurs in the two rather simple and still idealised stellar wind systems. In the more realistic situation, the variability would be enhanced further because we expect (i) yet smaller number of wind sources, (ii) a more diverse set of stars with different mass loss rates, (iii) non-circular stellar orbits, (iv) intrinsic stellar wind variability for luminous blue variable stars, etc.

4 FAST AND SLOW (TWO-PHASE) WINDS

The next ingredient we add to our treatment of accretion of stellar winds on to Sgr A* is the presence of slow winds. Previous models have considered only wind velocities $\gtrsim 600$ km s^{-1}, as measured by Najarro et al. (1997). However, Paumard et al. (2001) showed that several of the inner stars with important mass-loss rates emit winds with velocities as low as ~ 200 km s^{-1}. This has important consequences, because the slow winds are expected to cool and form clumps (Cuadra et al. 2005).

We use 20 wind sources in total, with each star loosing mass at the rate of $\dot{M}_* = 4\times10^{-5}\,\mathrm{M}_\odot$ year^{-1}. To resemble the two observed populations of luminous blue variable candidates, 'LBVs', and Wolf–Rayet stars, 'WRs', we assume that stars in our simulations can have either $v_\mathrm{w} = 300\,\mathrm{km\,s^{-1}}$ or $v_\mathrm{w} = 1000$ km s^{-1}, characteristic values for the two populations respectively. The values for the inner and outer boundary conditions are $R_\mathrm{in} = 0.07''$ and $R_\mathrm{out} = 9''$. We run the simulations for $\approx 4,000$ yr, then the number of particles reaches $N_\mathrm{SPH} \approx 1.5\times10^6$.

For the distribution of the stars we adopt two different configurations. First, we place the stars into two discs in order to reproduce the distribution reported by Genzel et al. (2003). We also place most of the LBVs in the inner disc, following Paumard et al. (2001). However, the stellar orbits are still only roughly known and the latest observations suggest that the LBVs may actually be distributed more evenly among both stellar systems (Genzel, priv. comm.). For these reasons, we consider a second simulation where the stars are distributed isotropically. The real distribution of the mass-loosing stars should be somewhere in between these two extreme cases.

The simulations presented here differ from the work of Cuadra et al. (2005) in that we do not split particles that get relatively close to the SMBH. The splitting was used to increase the resolution in the inner part. However, further tests showed that some loss of accuracy can occur in our present implementation of this approach, so that it failed to really show a convincing practical advantage.

4.1 Stellar wind sources placed in two discs

Here we attempt to model the Sgr A*–stellar wind system by setting up the stellar source distribution in a way that resembles the observations of the inner parsec in the GC (Paumard et al. 2001; Genzel et al. 2003). Our approach is the same as the one described by Cuadra et al. (2005), therefore we describe it only briefly here.

The stars are distributed uniformly in radius and in two perpendicular rings. All stars follow circular Keplerian orbits. The radial extent of the rings is from $2''$ to $5''$ and $4''$–$8''$ for the inner and outer one respectively. Out of the 20 wind sources, we assume that 6 LBV-type and 2 WR-type stars are in the inner ring, and the outer ring is populated by 3 LBVs and 9 WRs.

4.1.1 Large scale structure of the gas flow

Figure 7 shows the resulting morphology of the gas 2.5 thousand years into the simulation. The inner ring, mainly composed of LBVs that are shown by asterisks, is viewed face-on in the left panel, and edge-on in the right one. The inner ring stars are shown with the red coloured symbols whereas the outer disc stars are painted in black. The inner stars are rotating clock-wise in the left panel of the figure, and the outer ones rotate counter clock-wise in the right panel.

Cool dense regions in the gas distribution (shown as bright yellow regions in Fig. 7), are mainly produced by winds from LBVs. When shocked, these winds attain a temperature of only around 10^6 K, and, given the high pressure environment of the inner parsec of the GC, quickly cool radiatively (Cuadra et al. 2005). LBV winds form bound clouds of gas, often flattened into filaments due to the SMBH potential and the symmetry of the problem. As more filaments are formed in the inner region, they start overlapping and eventually form a disc that lies almost at the plane $z = 0$. The orientation of the disc plane is very close to that of the inner stellar ring, which at first may appear surprising given that there are 3 other LBV stars at the larger stellar disc. However, the escape velocity from the outer ring is of the order of the stellar winds velocity for the LBVs, and thus a large fraction of the slow wind from the outer ring escapes the computational domain and never influences the inner cold disc orientation.

The fast winds contribute to the inhomogeneity of the cold gas. This is well illustrated by one of the two WR-stars placed in the inner ring at $(x, y) \approx (2, 2.5)$ in the right panel of Fig. 7. The wind from this star has more mechanical power than all of the winds from the other LBVs in the simulation ($L_{\rm mech} \propto \dot{M}_* v_{\rm w}^2$). It cuts the combined wind of four neighbouring LBVs into two bands of gas. These two streams of gas are further stretched out by tidal shear from the SMBH and then chopped into smaller cool blobs by the interaction with the winds of the outer ring.

The three LBVs placed in the outer ring add complexity to the morphology of the cool gas as they produce cool gas streamers moving in a plane different from that of the inner one. One of these stars is at $(x, z) \approx (-5.5, -1)$. It produces most of the cool blobs of gas seen at the left of the right panel. Also note that the LBV at $(x, z) \approx (4, 1)$ is uplifting a significant amount of the cooled wind from the inner LBVs. On the other hand, the WRs by themselves do not produce much structure, as seen for instance from the two stars located at the upper left corner on the right panel. The fast winds they produce have temperatures $\gtrsim 10^7$ K after shocking, and do not cool fast enough to form filaments.

Figure 8 shows the average gas temperature in a slice $z = \pm 0.5''$ (left panel) and in a slice $y = \pm 0.5''$ (right panel) of the inner $6''$ region[3]. The clumps and the disc are cold as a result of radiative cooling, and before they collide the stellar winds have a low temperature as well. However, close to the stars the temperature appears higher than it would have been in reality. This is an artifact of the injection of a finite number of SPH particles per time-step into the wind, which creates some small-scale structure in the density and pressure profiles, leading to energy dissipation. This effect is however of minor importance since the temperature in these regions is still relatively low compared to the maximum temperatures that the gas can attain in a shock. In other words, the energy of the winds is still strongly dominated by the bulk motion of the gas rather than thermal energy.

The diffuse gas filling up the rest of the space is hot, with temperature $\sim 10^7$ K, comparable to that producing X-ray emission detected by *Chandra*. Gas cooler than that would be invisible in X-rays due to the finite energy window of *Chandra* and the huge obscuration in the Galactic plane.

4.1.2 Structure of the inner flow

Figure 9 depicts the structure of the inner flow later in the simulation, at $t = 4.0 \times 10^3$ years. At this late time, the cool disc becomes heavier and larger in the radial direction than seen in Fig. 7. The inner $\sim 0.3''$ region is still devoid of cool gas except for a few filaments. This is due to two reasons. First, the angular momentum of the slow winds from the innermost stars is not zero, even for the wind directed in the opposite direction of the stellar motion. The Keplerian circular velocity at $2''$ is $v_{\rm K} \approx 440$ km/sec, whereas the wind velocity is $v_{\rm w} = 300$ km/sec. Thus wind with even the minimum angular momentum would circularise at $r \sim 2'' \times (v_{\rm K} - v_{\rm w})^2 / v_{\rm K}^2 \sim 0.2''$. However, due to interactions of this gas with the gas with higher angular momentum, the minimum disc radius is actually a factor of ~ 2 higher. Second, the inner empty region of the disk is not filled in by the radial flow of cold gas through the disc because the viscous time scale of the cold disc is enormously long compared with the duration of the simulation (e.g. Nayakshin & Cuadra 2005). Gas clumps having low angular momentum infall into the inner arcsecond, but this does not occur frequently enough to fill in that region, and most of these clumps appear to be disrupted and heated in collisions. The long viscous time-scale is also the reason why the filaments do not merge forming a smooth disc at larger radii. The individual filaments that give shape to the disc are still distinguishable in the figure.

The mass of the cold disc is actually quite small, i.e. only $\approx 0.2\,{\rm M}_\odot$. It is instructive to compare this number with the mass of the wind produced by the 'LBV' stars in 4×10^3 years, which turns out to be $1.4\,{\rm M}_\odot$ for this simulation. Obviously most of the cold gas escapes from the simulation region. However, some of this gas does not have a true escape velocity. Had we simulated a larger region, a fraction of this cold gas could return to the inner region on highly eccentric orbits, producing further variability and complexity in the morphology of the cold gas and accretion history of Sgr A*.

*4.1.3 Accretion on to Sgr A**

As described in Section 2, all gas particles entering the inner boundary of the computational domain, in this case $R_{\rm in} = 0.07''$, are presumed to be instantaneously accreted by Sgr A*. In practice, such accretion would happen on the viscous time scale of the flow, which depends on the viscosity α-parameter (Shakura & Sunyaev 1973), the gas temperature and the circularisation radius. When taking these factors into account, we would expect a time-scale of at least

[3] To avoid low-density hot regions from dominating the map, we column-averaged $\log T$ rather than simply T.

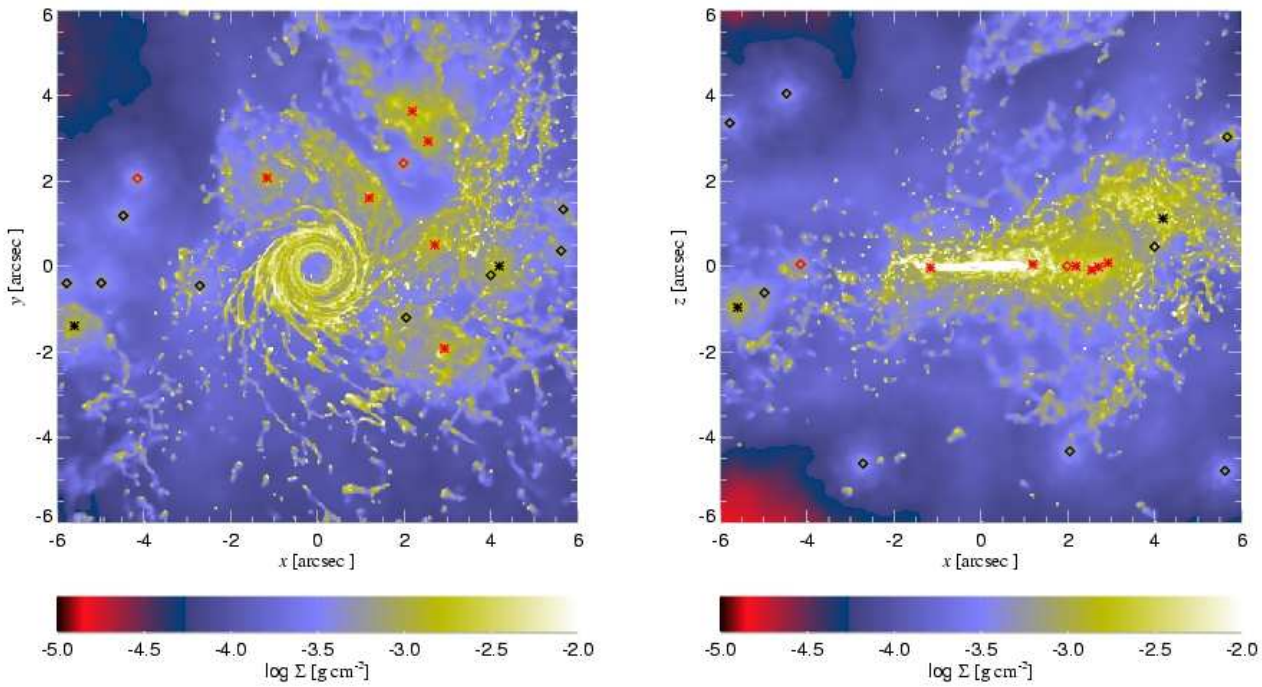

Figure 7. Left panel: Column density of gas in the inner $6''$ of the computational domain 2,450 years after the beginning of the simulation. Stars of the inner disc are shown as red symbols, while the ones on the outer disc appear in black. Asterisks mark slow wind stars (LBVs), whereas diamonds mark stars producing fast winds (WRs). The inner stellar ring is face-on while the outer one is seen edge-on (plane $y = 0$). Right panel: same as on the left, but the outer stellar ring is now seen face-on while the inner one appears edge-on ($z = 0$).

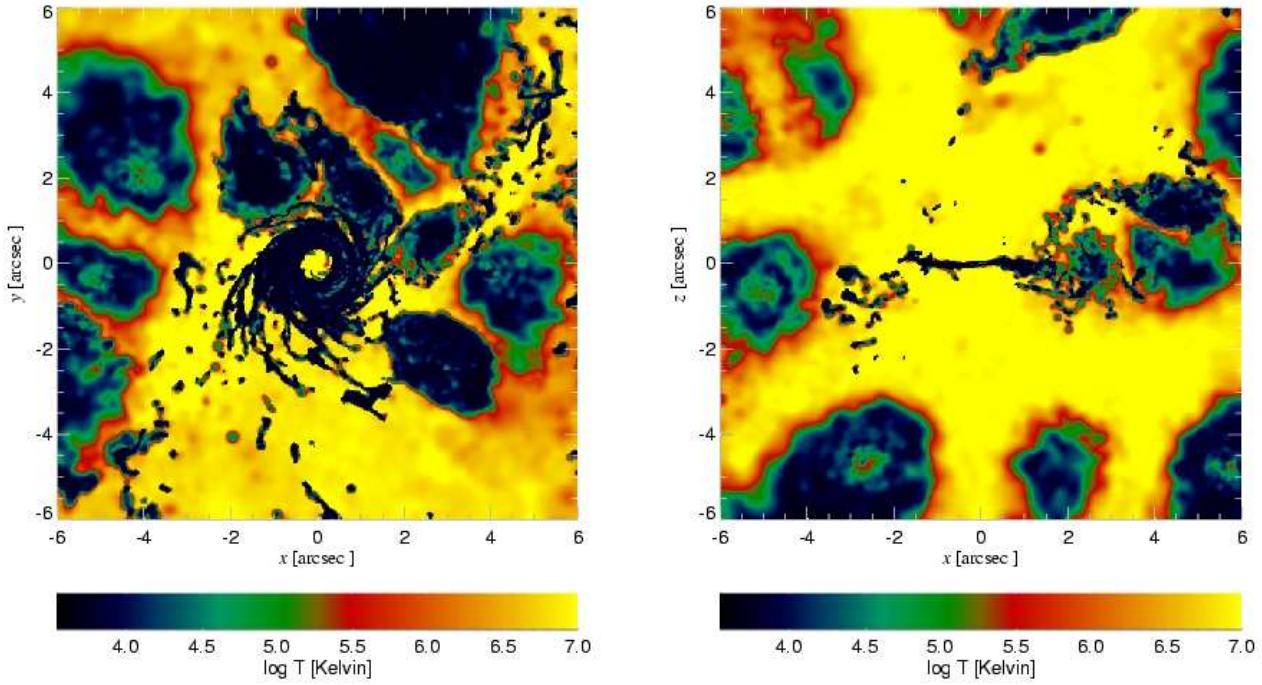

Figure 8. Similar to Fig. 7, but showing $1''$-thick cuts of the gas temperature. Stars are not shown for clarity. The left panel shows a slice between $z = -0.5''$ and $+0.5''$, whereas the right one shows the gas temperature in the range $-0.5'' < y < +0.5''$. The minimum temperature in the simulation is set to 10^4 K. In reality gas would cool even further, likely to a few hundred K.

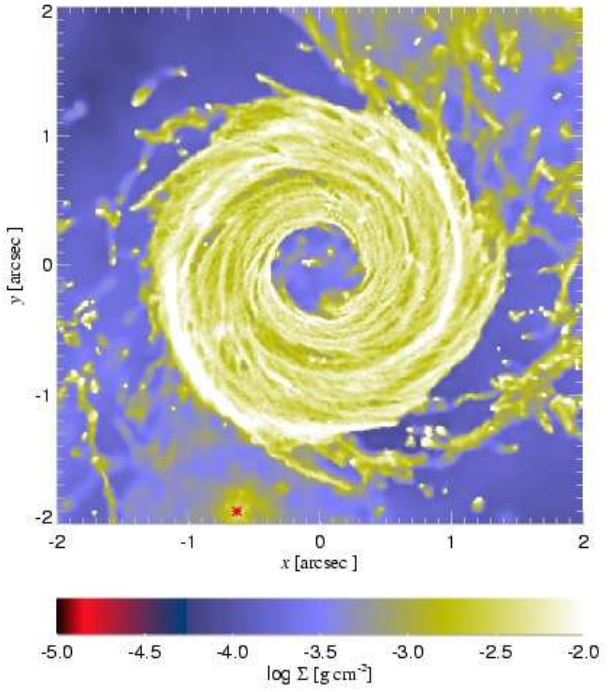

Figure 9. Top view of the inner 2″ cube at time $t = 4.0 \times 10^3$ years. Note that the disc grew larger in radial extent but the inner region is still devoid of cool gas except for a few clumps.

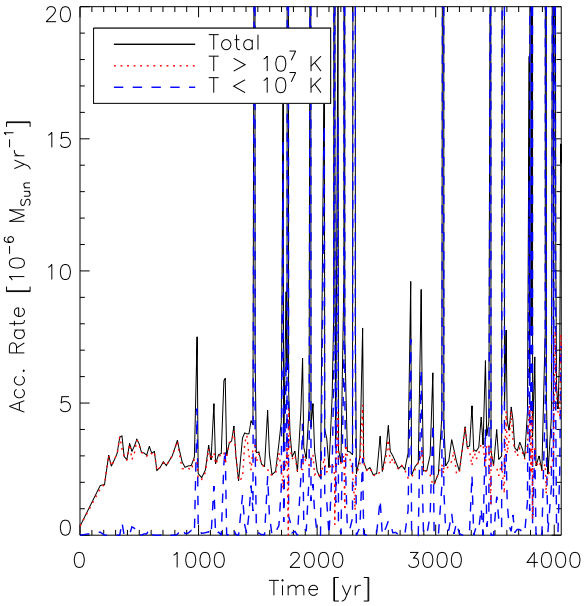

Figure 10. Accretion rate on to the SMBH as a function of time (black line). This rate is then divided into that of hot gas (red) and that of low temperature gas (blue). Note that the time-averaged accretion is dominated by the hot component that is quasi-constant; the accretion of cold gas is episodic and highly variable, but smaller overall.

10 yr for the accretion of hot gas. For this reason, in Fig. 10, we plot the accretion rate smoothed over a time-window of duration $\Delta t \approx 10$ years.

Figure 10 also shows the accretion rate of hot ($T > 10^7$ K, red line) and cold ($T < 10^7$ K, blue line) gas separately. The accretion rate of hot gas is fairly constant, and has a value $\dot{M}_{\rm BH} \approx 3 \times 10^{-6}\,{\rm M}_\odot\,{\rm yr}^{-1}$, consistent with the *Chandra* estimates (Baganoff et al. 2003). In addition to this component, the intermittent infall of cold clumps produces most of the variability in the accretion rate. The cold gas falls into the innermost regions due to two factors: (i) it is initially created on low angular momentum trajectories, and/or (ii) it acquires such orbits through collisions with other cold gas clumps.

For further analysis we define the local mass inflow and outflow rates integrated on shells at a given radius. Figure 11 shows both of these quantities, for all the gas (thin lines), and for the hot gas only ($T > 10^7$ K, thick lines). The profiles were measured in a similar fashion as those in Section 3 by stacking 10 snapshots at $t \approx 2.5 \times 10^3$ yr. For the hot gas, the outflow practically cancels the inflow between 0.4″ and 2″. Only the gas with low enough angular momentum and thermal energy accretes in this region, the rest escapes into the outflow. This effect is completely absent in a spherically symmetric flow such as the Bondi (1952) solution.

The true accretion flow in our simulation starts at $R \approx 0.4''$, where the inflow rate becomes approximately constant and the outflow is negligible. This radius would be a better definition of the effective capture radius.

The profiles that include all the gas (thin lines) are dominated by cold gas in the disc at $R \approx 0.3$–$1.3''$. We find that

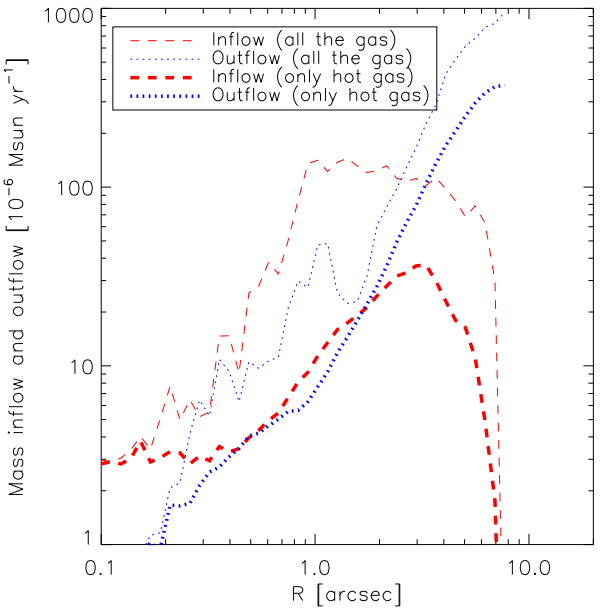

Figure 11. Mass inflow (red curves) and outflow (blue) as a function of radius. The thick lines show the profiles for the hot gas only, while the thin lines include all the gas.

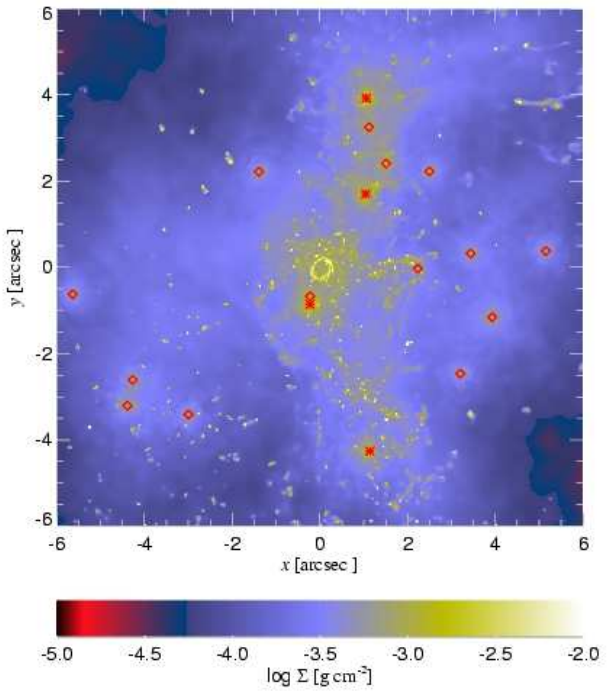

Figure 12. Gas column density map for a simulation with 20 stars, chosen as in Section 4.1 but with orbits that have a random angular momentum vector.

the mean eccentricity for this gas is $e \approx 0.1$. This deviation from circular velocity, together with the relatively high mass of the disc explain the 'noise' in the inflow/outflow profiles in this region. However, the inflow dominates, and its net rate is much larger than the accretion rate at $R_{\rm in}$, so an important fraction of the gas actually stays in the disc, making it grow in mass. For larger radii the inflow becomes negligible and the outflow rate reaches approximately the total mass loss rate of the wind sources, $\dot{M}_{\rm w} = 10^{-3}\,{\rm M}_\odot\,{\rm yr}^{-1}$.

4.2 Simulation with isotropic orbits

With the aim to test how the results depend on the assumed stellar orbits we run a simulation with exactly the same set-up as in the previous subsection, but instead of placing the stars into the two rings, we oriented the stars' circular orbits randomly. The distribution of angular momentum vectors is obviously isotropic for this case.

Figure 12 shows the column density of the gas at $t = 2.4\times10^3$ years after the beginning of the simulation. For this simulation, no conspicuous disc is formed. Instead, we find that only a small ring on scales of $\sim 0.5''$ is formed. The ring has the same angular momentum direction than the innermost star (an LBV). Its radial scale is smaller than the inner boundary of the disc formed in Section 4.1.2, because in this simulation the gas that formed the ring interacts with a larger quantity of gas with different angular momenta, loosing its own.

4.3 Comparison of both simulations

The prominent disc-like structure that we find in the simulation with two stellar discs appears to be inconsistent with some of the current observations. In infrared images (e.g., Scoville et al. 2003; Paumard et al. 2004) complex structures of cold gas are indeed seen, but they are not in a disc configuration. In addition, the cold gas structures are typically observed on larger scales than what we find in our simulation. The most likely reason for the discrepancies between these recent observations and our model may be ascribed to the specific initial conditions we used. In particular, placing many LBVs in the same plane at a short distance from the SMBH may be particularly favourable for the development of a disc. Completely different is the case in which the stellar orbits are oriented randomly (Section 4.2). The distribution of angular momenta vectors is obviously isotropic for this case, so there is no obvious preference for a particular plane where a disc would form. The tiny ring formed there perhaps could be missed observationally or not formed at all if closest slow wind stars are in reality farther away than we assumed for the simulation.

Nevertheless, in both simulations we get a two-phase medium in the inner region, and a comparable accretion rate. These are robust results, dependent only on the velocities we have chosen. The specific gas morphology, instead, depends strongly on the orbital geometry of the initial source distribution.

The angular momentum profiles (defined as in Section 3.2) of gas in the simulations with isotropic orbits (blue) and with two discs (red) are shown in Fig. 13. In the isotropic case the angular momentum is low at the wind source region. In contrast, the gas angular momentum is much higher in the two stellar disc simulations at the same range of radii. Somewhat surprisingly, the angular momentum content of hot gas in the inner arcsecond is actually quite similar for the two simulations. This can be traced to the hydrodynamical interaction of the hot gas with the cold gas, whose net angular momentum is much higher. Indeed, the angular momentum profiles of all the gas (cold and hot), shown with thin curves in Fig. 13, are nearly Keplerian in the inner arcsecond region.

4.4 Comparison of the two-phase and one phase simulations

At this point it is also instructive to highlight some of the systematic differences between the 'one-phase' (fast winds only) and the 'two-phase' simulation results. The angular momentum profiles of the one-phase and two-phase simulations are shown in Figs. 4 and 13, respectively. While in the one-phase simulations the angular momentum of gas near the capture radius was always much lower than the local Keplerian value, the two-phase simulations show almost Keplerian rotation near the inner boundary. As explained in Section 4.3, this is caused by the interaction between the hot and the cold gas phases. Only the part of the fast wind that has a low angular momentum accretes from the hot phase, because its pressure support against SMBH gravity is already high. In contrast, cold gas has little pressure support and hence even gas with a rather high angular momentum can be captured into the central arcsecond by Sgr A*. This

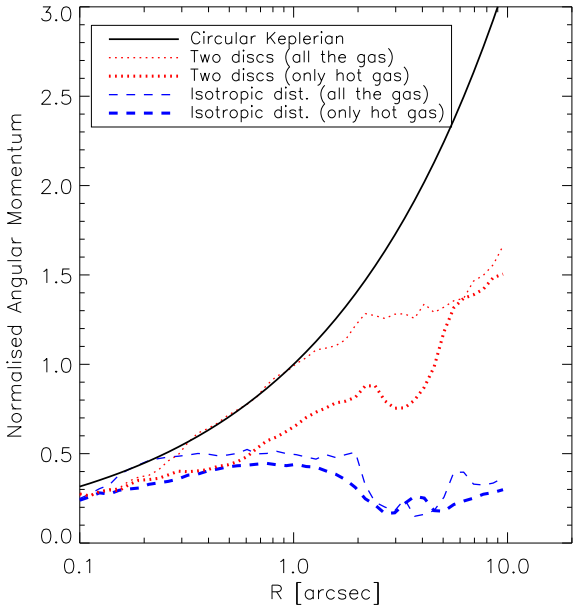

Figure 13. Angular momentum profiles of the simulations with isotropic orbits (blue, Section 4.2) and with two discs (red, Section 4.1). For comparison, the value of a Keplerian circular orbit is shown as well (black line).

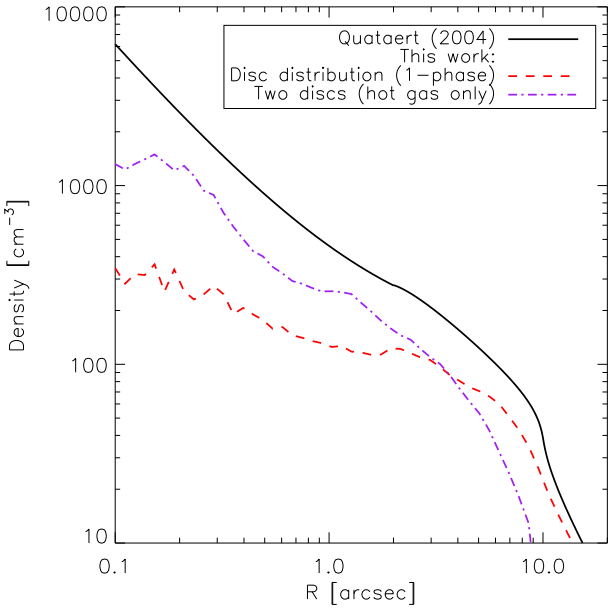

Figure 14. Hot gas density profiles of 'one-phase' simulations with stars arranged in disc orbits (red dashed line, Section 3.2) and two-phase simulations with two discs of stars (violet dot-dashed, Section 4.1). Note that the two-phase simulation yields a much more centrally concentrated profile.

also implies that such two-phase accretion flows are more strongly rotating, or more precisely, that their circularisation radii are larger (see Section 6.5).

The other notable difference between the one and two phase simulations is that the latter produce much more concentrated radial density profiles for hot gas (Fig. 14). Due to the presence of slow winds and thus more prominent radiative cooling, the two-phase simulations yield less pressure support for the gas. A larger angular momentum is then needed to support the gas against gravity, as pointed out above. However this extra support is apparently insufficient and the radial density profile plunges in quicker in the two-phase case than it does in the one phase case. Interestingly, despite using a different setup and including different physics, our two-phase hot gas density curve is by and large similar in shape to that of Quataert (2004), although yielding a lower accretion rate.

5 WHAT WOULD CHANDRA SEE?

Having obtained maps of the gas density and temperature distributions, we calculate the expected X-ray emission of each pixel. We use an optically thin cooling function $\Lambda(T)$ (see Section 2), modified to crudely model the effects of the interstellar absorption. As is well known, the column depth of the cold ISM to Sgr A* is very high, $N_{\rm H} \sim 10^{23}$ hydrogen atoms cm^{-2} (e.g., Baganoff et al. 2003), and hence *Chandra* receives hardly any photons with energy less than ~ 2 keV. Therefore, gas cooler than $T \sim 10^7$ Kelvin will contribute very little to the X-ray counts. We then use

$$\Lambda_{\rm mod}(T) = \frac{\Lambda(T)}{1 + (T_{\rm cut}/T)^5} \ , \qquad (1)$$

where $T_{\rm cut} = 10^7$ Kelvin. [4] Below we consider X-ray emission from two of our simulations.

Figure 15 shows a resulting X-ray map for the simulation with fast winds only (Section 3), with 40 stars in a rotating disc configuration. The map shows the luminosity (normalised to one arcsec) integrated over pixels of $0.5''$, which is about the *Chandra* pixel size (clearly we could have produced much finer simulated X-ray images of the GC). Remarkably, the density of the hot gas in the inner arcsecond is so low that stellar winds actually dominate the X-ray map. This is due to two factors. First, the stellar density is greater for stars located in a (relatively thin) disc than it is for the same stars spread around a spherical shell at the same radial distance. As a result, the stars are closer to each other and the shocked gas density is higher. Second, the large angular momentum of the gas prevents most of it from flowing into the inner arcsecond of this simulation (see Figs. 4 and 5), thus reducing the X-ray emission from the centre.

Figure 16 depicts the light curves of the radial annuli ($R < 1.5$, 3 and $6''$, respectively) for the simulation corresponding to Fig. 15. Clearly, the central region never dominates the X-ray emission. Also, variability is rather mild and occurs on time scales of hundreds of years.

Figure 17 shows the more 'realistic' simulation which includes both fast and slow winds with stars located in two rather than one ring. Note that the scale of the colour bar on the bottom is 10 times higher than that used in Fig. 15. In

[4] A very sharp rollover in temperature is justified by the very strong dependence of photo-electric absorption cross section on photon energy.

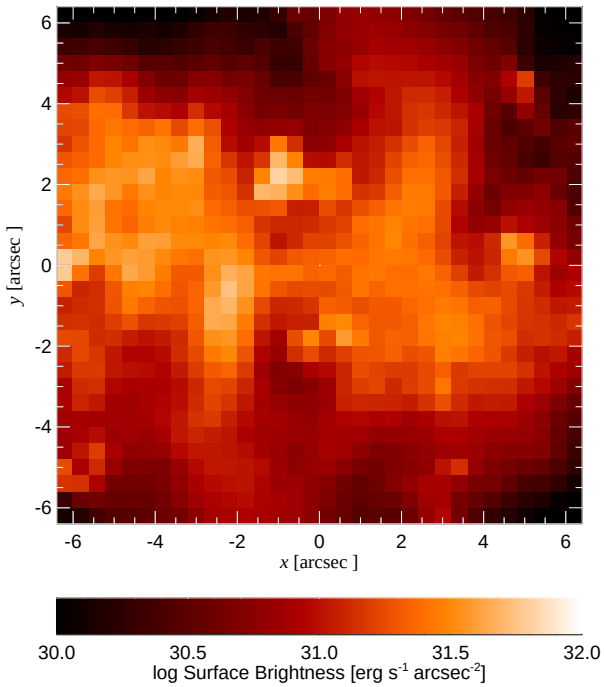

Figure 15. Simulated *Chandra* view of the inner 12″ by 12″ for the simulation with fast winds only (Section 3), with 40 stars arranged in a disc configuration. The corresponding density profile was shown in Fig. 5 (dashed red curve). Note the strong and highly extended emission from stellar wind shocks. No central source associated with Sgr A* is actually visible.

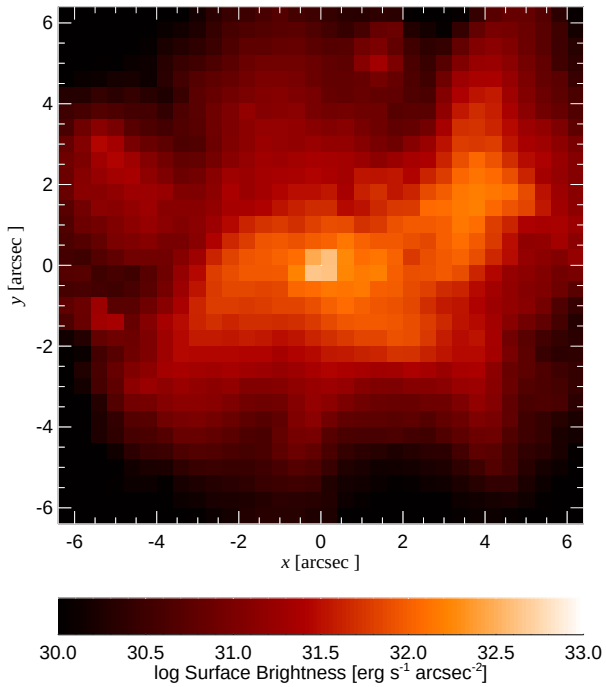

Figure 17. Simulated *Chandra* view of the inner 12″ by 12″ for the simulation shown in Fig. 7. The rings of stars are inclined at a 45° angle to the line of sight in this figure. Note that the central arcsecond clearly stands out in X-rays, but the emission is spatially extended, perhaps slightly more than in the real Sgr A* observations by *Chandra*.

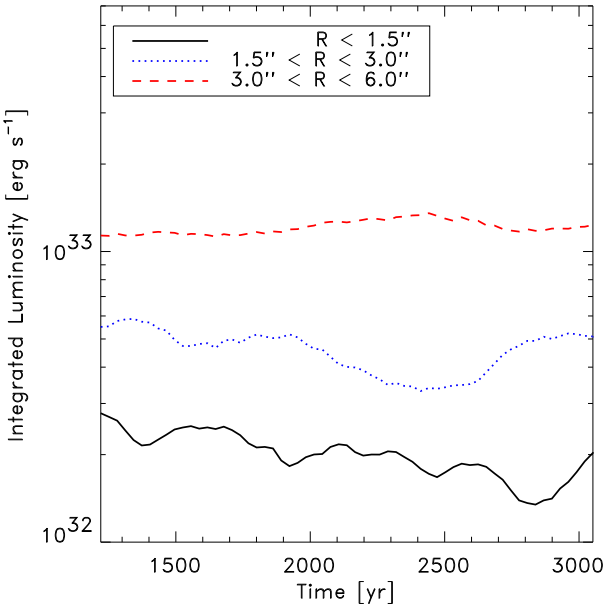

Figure 16. Light curves of three radially selected regions, as indicated in the inset. Variability is due to changes in the relative positions of the stars. The luminosity of the inner region is correlated with the accretion rate, because both are determined by the density in the inner arcsecond.

sharp contrast with Fig. 15, the central source clearly stands out now at a level consistent with that observed by *Chandra*. This difference is caused by a much stronger concentration of the hot gas in the centre in this latter model, discussed in Section 4.4.

Figure 18, shows the light curves corresponding to Fig. 17 and can be directly compared with Fig. 16. We note that in the more 'realistic' simulation the X-ray luminosity of the central source is higher and is by far more variable. The steady state X-ray emission is larger simply due to the higher hot gas density in the inner region, whereas the variability is produced by shock-heated blobs impacting the cold disc. During such events the peak in the X-ray intensity can actually shift from Sgr A* nominal position by $\sim 0.5''$ or so.

It would be interesting to compute the X-ray spectrum of each pixel, and then compare that to *Chandra* observations of Sgr A*. This would involve calculation of the local radiation spectrum, radiation transfer along rays and a model for X-ray absorption in the interstellar matter between the GC and us. We leave such a detailed comparison with observations for future work.

6 DISCUSSION

The theory of accretion flows on to SMBHs is an area of active research (e.g., Narayan 2002) where observational tests constitute strong drivers in the field. Due to its proximity, Sgr A* is the only SMBH where it is becoming possible to

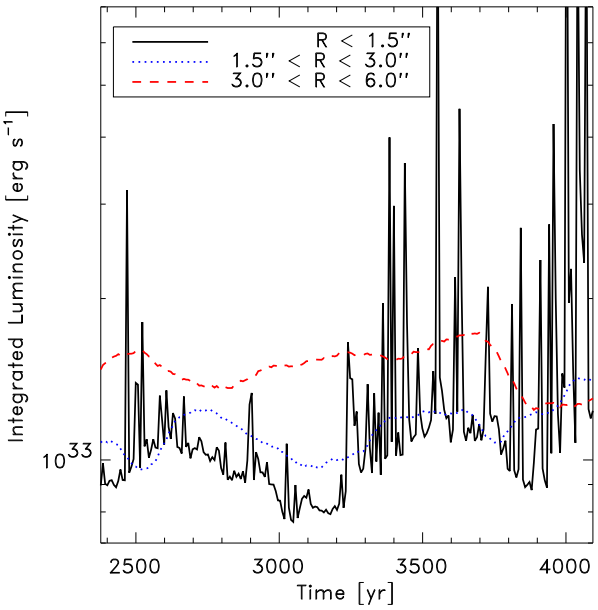

Figure 18. The same as for Fig. 16 but for the simulation with two rings of stars (see Fig. 17). Note that now the central region is brighter and much more variable. The variability in the light received from the central region is mainly caused by cool blobs of gas raining down on to the disc, shock-heating gas to X-ray emitting temperatures.

constrain observationally the accretion flow properties both at small and large radii simultaneously ($R \sim 10 - 100 R_{\rm S}$ and $R \sim 10^5 R_{\rm S}$; see Bower et al. 2003; Baganoff et al. 2003; Nayakshin 2005).

The most direct method to measure the accretion rate is through *Chandra* X-ray observations (Baganoff et al. 2003). However, this method has the following drawbacks: (a) gas cooler than $\sim 10^7$ K cannot be observed due to a very high neutral hydrogen absorbing column to the GC, thus the contribution of cool gas is unknown; (b) bulk motions of the gas can in principle make some of the gas unbound, but these do not directly enhance the X-ray emission, and thus they can be missed; (c) only the instantaneous conditions can be probed, whereas the relevant time scales can be tens and hundreds of years.

The second method to infer the input accretion rate is through observations of stellar winds and models of the outflows and gas accretion on to the SMBH. This method alleviates deficiencies (a-c) discussed above, but of course comes with its own set of problems and uncertainties. In this paper, we have attempted to reduce these in the part of the theoretical (numerical) modelling of the wind hydrodynamical evolution. Conceptually, we built on the previous numerical work in the area (Coker & Melia 1997; Rockefeller et al. 2004) and on the semi-analytic model of Quataert (2004). However, we have used a Lagrangian SPH/N-body code, allowing us to follow the problem in its full 3D setting. Compared with previous authors, we have been able to relax assumptions that stellar wind sources are fixed in space and that shocked winds suffer no radiative losses. We have also varied stellar orbital distributions, testing rotating disc-like and isotropic distributions.

6.1 Reduction of accretion due to anisotropy and net angular momentum

We performed three runs with fast stellar winds ($v_{\rm w} = 10^3$ km s^{-1}) produced by 40 stars. These runs tested the importance of the orbital motions and the source distribution. For a stationary spherical stellar distribution, the accretion rate (see Fig. 6) was found to be around $\sim 10^{-5}\,{\rm M}_\odot$ year^{-1}, with variability at a level of 10%. These results are consistent with that of Coker & Melia (1997) after correcting for small differences in wind velocities and stellar wind loss rates. Allowing the stars to follow randomly oriented circular Keplerian orbits decreased the accretion rate by a factor of three, and increased the variability up to $\sim 50 - 70\%$ (blue dotted curve in Fig. 6). Placing these same stars into a disc reduced the accretion rate by another factor of three or so, while keeping the variability magnitude at about the same level. The main driver of the differences in these three tests is the net angular momentum of the gas (Fig. 4). We find that only the gas with a low enough angular momentum makes it to the inner boundary and hence is accreted, and the fraction of such gas decreases when the source distribution is rotating with a common direction (a disc).

Another way to view this result is to say that the angular momentum of the gas and 'random' gas motions reduce the gas capture radius. Although authors' definition of the latter differ slightly, most consider the capture radius to be 1–2″ (Baganoff et al. 2003; Rockefeller et al. 2004), whereas we would define $R_{\rm capt}$ to be about 0.4″ based on our simulations. Indeed the gas can be called captured only at this region, where accretion (see Fig. 11) strongly dominates; at large radii outflow and inflow nearly cancel each other.

6.2 Cool phase of stellar winds

In a fixed pressure environment, gas cooling time is a very strong function of temperature: $t_{\rm cool} \propto T/(\Lambda(T)n) \propto T^2/\Lambda(T)$, where $\Lambda(T)$ is the optically thin cooling function, here dominated by metal line cooling. Further, shocked gas temperature is proportional to the initial velocity of the winds squared, v_w^2. Taking these facts together one finds that gas cooling time scales as $v_w^{5.4}$ (Cuadra et al. 2005, eq. 2). Therefore, for the Wolf-Rayet winds, with velocities of a thousand km s^{-1}, gas cooling time is much longer than the dynamical time and the effect of cooling is negligible. However, for outflow velocity of 300 km s^{-1}, radiative cooling is faster than the local dynamical time. We therefore find that these winds cool radiatively and form clumps of cold gas.

We find that cold clumps form independently of the geometry of the stellar system, as long as wind velocity is low enough. The morphology of cold gas however strongly depends on the orbital distribution of slow wind sources. In Section 4 we tested two extreme cases for the stellar distribution: stars in two discs, and in a spherically symmetric system. An extended cold disk was present in the former configuration, and only a tiny gas ring in the former.

A detailed comparison between the gas morphology in our simulations and in the observations is beyond the scope

of this work. However, it is interesting to note that the radio images presented by Wardle & Yusef-Zadeh (1992) show an asymmetry in the gas that these authors attributed to the influence of stellar winds. This anisotropy suggests that the stellar wind sources are not distributed isotropically, whereas the absence of a conspicuous disc points out that the narrow line stars of the inner few arcsec have different orbital planes.

Eckart & Morris have recently reported[5] the presence of extended mid-infrared emission blobs. Their red spectrum is interpreted as dust emission. It is possible that some of these blobs were actually formed from the stellar winds as in our simulations. Since for the slow winds in our simulations cooling is important, and since the gas would probably cool much further than the minimum temperature of 10^4 K assumed here, formation of dust would follow. One of the observed blobs is only $0.026''$ away from Sgr A* in projection and is probably responsible for the offset between the dynamical centre and the Sgr A* mid-infrared emission detected by Clénet et al. (2004). Monitoring its proper motion will show whether it is physically close to Sgr A* and therefore if it could be identified with one of the clumps that feed the SMBH in our simulations.

Finally, radio observations (Yusef-Zadeh et al. 1998) have revealed the presence of clumps with proper motions high enough to escape from the GC region. The mass of one of them, 'the bullet', is estimated at $8\times10^{-4}\,\mathrm{M}_\odot$. This mass is of same order as the typical mass of cold clumps leaving the inner region in our simulations.

6.3 Long term evolution of the disc

In Section 4.1 we stopped the simulation after ~ 4000 yr. At this point the total mass of cold gas keeps growing in the inner few arc-seconds and there is no obvious tendency for reaching a steady state. However, because of factors not included in the simulation, it is very likely that in a few thousand years the disc would be destroyed. One reason for that is the presence of many massive stars that would explode as a supernova (SN) within a short time-scale. There are currently tens of WR stars in the GC star cluster. This stellar phase is expected to last a few $\times10^5$ yr, at the end of which the star explodes as a SN. Therefore a SN explosion is expected every $\sim 10^4$ yr.

Let $R_{\rm sn}$ be the distance between a supernova and Sgr A*, and $E = 10^{51}E_{51}$ erg s^{-1} be the total energy content of the supernova shell. The disc material will then be accelerated to a velocity $v_{\rm acc}$ given by $\Sigma_{\rm disc}v_{\rm acc}^2 \sim E_{\rm sn}/4\pi R_{\rm sn}^2$. For example, for disc radius $R_{\rm disc} = 2''$, the ratio of this velocity to the local Keplerian velocity is

$$\frac{v_{\rm acc}^2}{v_{\rm K}^2} \sim 1\,\frac{E_{51}}{M_{10}R_{10}^2}\,, \qquad (2)$$

where $R_{10} = R_{\rm sn}/10''$ and $M_{10} = \pi\Sigma_{\rm disc}R_{\rm disc}^2$ in units of 10 $\mathrm{M}_\odot$. This shows that a supernova occurring within the inner 0.5 pc of the Galaxy would destroy the disc. A fraction of the disc with the lowest angular momentum would likely be captured by the SMBH and would result in a bright flare that would last at least a few hundred years, the dynamical time at a couple of arc-seconds distance from Sgr A*. Such flares may be responsible for the X-ray/γ-ray echo of Sgr A* recent activity on nearby giant molecular clouds, most notably Sgr B2 (Sunyaev et al. 1993; Koyama et al. 1996; Revnivtsev et al. 2004), and the observed plumes of hot gas also indicative of former AGN activity (Baganoff et al. 2003).

Another factor that should be taken into account for a realistic simulation on longer time-scales is the presence of the 'mini-spiral'. This seems to be a collection of infalling gas structures, with masses of dozens of $\mathrm{M}_\odot$ (Paumard et al. 2004). Since their orbital time-scales are a few $\times10^4$ years, by that time collisions between these structures and the disc are expected, resulting in the destruction or a significant rearrangement of the latter. Again this would enhance the accretion rate on to Sgr A*.

6.4 Variability

We have shown that adding more realistic ingredients in our simulations introduces substantial variability into the accretion rate on to Sgr A*. In Section 3.2, with 40 identical stars, the variability increased from less than $\sim 10\%$ to about 50% by just allowing the stars to follow circular orbits (Fig. 6). Further, in Section 4.1, the inclusion of slow stellar winds led to the formation of cold clumps. The accretion of these clumps proceeds in short bursts, producing a highly variable transfer of mass into the inner $0.1''$ (Fig. 10). The actual rate of accretion on to the SMBH has still to be determined by the accretion flow physics that we cannot resolve here, but it is expected to maintain most of the variability in time-scales longer than ~ 100 yr.

There are additional sources of variability that have not been included in our treatment. Some of the stars with high outflow rates probably have orbits with a non-negligible eccentricity. Then the fraction of winds that can be captured from a given star by the black hole changes with time. In addition, there could be intrinsic variability of the stars themselves. LBVs outside the GC have been observed to vary their mass-loss rates by more than an order of magnitude within a few years (e.g., Leitherer 1997). In the GC, the line profiles of IRS 16 NE & NW have changed in the last few years. This is usually attributed to orbital acceleration, but it could be partially caused by changes in the winds properties (Najarro, priv. comm.). Variability can also be produced by close X-ray binaries. Recently, Muno et al. (2005) and Porquet et al. (2005) identified a transient source located within 0.1 pc of the GC as a low-mass X-ray binary. Bower et al. (2005) detected its radio counterpart, and argue that it is the signature of a jet interacting with the dense gas of Sgr A West. Such a jet can influence the kinematics of the gas, and in some cases could drive material to the black hole vicinity. Finally, as we noticed in the previous subsection, SNe or the infall of cold gas from larger scales could lead to a strong increase in the accretion rate.

In the extreme sub-Eddington regime of Sgr A* accretion, the dependence of the luminosity on the accretion rate is very non-linear (see e.g., Yuan et al. 2002). Thus, even small changes in the accretion rate could result in a strongly enhanced X-ray emission. The results from our simulations, the observational evidence for higher luminosity in the re-

[5] KITP Conference on the GC, talks available online at http://online.kitp.ucsb.edu/online/galactic_ c05 .

cent past (Sunyaev et al. 1993; Koyama et al. 1996; Revnivtsev et al. 2004), and the idea of star formation in an AGN-like accretion disc a few million yr ago (e.g., Levin & Beloborodov 2003; Nayakshin & Cuadra 2005), all suggest that on long time-scales Sgr A* is an important energy source for the inner Galaxy.

6.5 Circularisation of the flow

The degree to which accretion flows are rotating is very important for theoretical models of these flows. For example, Melia (1992, 1994) assumes that gas inflows in essentially a quasi-spherical (Bondi 1952) manner down to a circularisation radius of $R_{\rm c} \sim 100 R_{\rm S}$, whereas, e.g., Narayan (2002) and Yuan et al. (2003) assume that the flow is strongly rotating already at a sub-arcsecond region. Recent detailed hydro and MHD simulations of Proga & Begelman (2003a,b) confirmed that the nature of the accretion flow strongly depends on the angular momentum of the gas at the outer boundary of the flow.

Here we find that in all of our simulations the accretion flows posses a relatively large angular momentum, and that in the two-phase wind simulations it is larger than in the one phase case. In terms of circularisation radii for the flows, we find $R_{\rm c} \sim 0.01'' \sim 10^3 R_{\rm S}$ for one-phase winds, and $R_{\rm c} \sim 0.1'' \sim 10^4 R_{\rm S}$ for two-phase flows. Physically, one-phase flows are hotter, and any significant rotation unbinds the gas in the inner arcsecond. This works as a surprisingly effective selection criterion for determining which particles do accrete, so in our one-phase simulations the gas in the inner region has roughly the same angular momentum, independent of the stellar motion.

On the other hand, in the two-phase simulations (fast and slow winds), radiative cooling of denser regions reduces the mean temperature of the gas. As a result, less pressure support is available for the gas, and the 'selection' criterion does not operate anymore. These flows rotate at almost the local circular Keplerian velocity near the inner boundary of our simulations. Remarkably, this result (for the hot gas) is largely independent of the orbital distribution of the stellar wind sources. Therefore, unless the mass loss rates of the slow (narrow line) wind stars are grossly over-estimated observationally, we conclude that weakly rotating accretion flows are unlikely to form in Sgr A*.

7 CONCLUSIONS

In this paper we presented a detailed discussion of our new numerical simulations of wind accretion on to Sgr A*. Compared with previous works, our methodology includes a treatment of stellar orbital motions and of optically thin radiative cooling. While the results are strongly dependent on the assumptions about stellar mass loss rates, orbits, and wind velocities, some relatively robust conclusions can be made.

Unless mass loss rates of narrow line mass losing stars (Paumard et al. 2001) are strongly over-estimated, the gas at $r \sim 1''$ distances from Sgr A* has a two-phase structure, with cold filaments immersed into hot X-ray emitting gas. Depending on the geometry and orbital distributions in the mass-loosing star cluster, the cold gas may be settling into a coherent structure such as a disc, or be torn apart and heated to X-ray emitting temperatures in collisions. Both the fast and the slow phase of the winds contribute to the accretion flow on to Sgr A*. The accretion flow is rotating rather than free-falling in sub-arcsecond regions, with a circularisation radius of order $10^4 R_{\rm S}$. The accretion rates we obtain are of the order of $3 \times 10^{-6}\,{\rm M}_\odot$ year^{-1}, in accord with the *Chandra* observations (Baganoff et al. 2003). The accretion of cooler gas proceeds separately via clump infall and is highly intermittent, although the average accretion rate is dominated by the quasi-constant inflow of hot gas. As is true for the hot gas, most of the cold gas outflows from the simulated region. However some of this gas is bound to Sgr A*, and, had we resolved a larger region, would come back into the inner regions on eccentric orbits.

A generic result of our simulations is the large variability in the accretion rate on to Sgr A* on time scales of the order of the stellar wind sources orbital times (hundreds to thousands years). Even in the case of one-phase flows the accretion rate shows variability by factors of a few. Simulations including more diverse populations of winds and stellar orbits, the presence of the single, very important mass-loosing star cluster IRS13 (Maillard et al. 2004; Schödel et al. 2005), or the observed ionised (e.g. $T \sim 10^4$ K) gas, can all be expected to further increase the time-dependent effects. This implies that the current very low luminosity state of Sgr A* may be the result of a relatively unusual quiescent state. It also means that the real time-averaged output of Sgr A* in terms of radiation and mechanical jet power may be orders of magnitude higher than what is currently observed. The role of Sgr A* for the energy balance of the inner region of the Galaxy may therefore be far more important than its current meager energy output would suggest. Observations of γ-ray/X-ray echos of past activity of Sgr A* (e.g., Revnivtsev et al. 2004) seem to confirm these suggestions from our simulations.

Further improvements in the models of wind accretion on to Sgr A* will benefit most strongly from better observational constraints on the properties of the stellar winds in the central parsec of the Galaxy. Future numerical improvements may be a higher dynamical range between $R_{\rm in}$ and $R_{\rm out}$, a larger number of SPH particles, and inclusion of magnetic fields. The latter are now believed to be very important for gas angular momentum transport via generation of the magneto-rotational instability (e.g., Balbus & Hawley 1991). At the same time, we expect angular momentum transport to be important only inside or close to the circularisation radius, i.e. somewhere near our inner boundary.

ACKNOWLEDGEMENTS

JC acknowledges D. Šijački and C. Scannapieco's help during his first attempts to use GADGET-2. We thank E. Quataert for sending us data files from his calculations and the anonymous referee for useful suggestions. Finally, this work benefited from discussions with the members of the GC group at MPE, especially R. Genzel and T. Paumard, and with F. Baganoff, M. Morris, F. Najarro and F. Yusef-Zadeh.

REFERENCES

Baganoff F. K., Maeda Y., Morris M., et al., 2003, ApJ, 591, 891
Balbus S. A., Hawley J. F., 1991, ApJ, 376, 214
Blandford R. D., Begelman M. C., 1999, MNRAS, 303, L1
Bondi H., 1952, MNRAS, 112, 195
Bower G. C., Roberts D. A., Yusef-Zadeh F., et al., 2005, ApJ, in press, astro-ph/0507221
Bower G. C., Wright M. C. H., Falcke H., Backer D. C., 2003, ApJ, 588, 331
Clénet Y., Rouan D., Gratadour D., et al., 2004, A&A, 424, L21
Coker R. F., Melia F., 1997, ApJL, 488, L149
Cuadra J., Nayakshin S., Springel V., Di Matteo T., 2005, MNRAS, 360, L55
Di Matteo T., Springel V., Hernquist L., 2005, Nature, 433, 604
Genzel R., Hollenbach D., Townes C. H., 1994, Reports on Progress in Physics, 57, 5, 417
Genzel R., Schödel R., Ott T., et al., 2003, ApJ, 594, 812
Ghez A. M., Duchêne G., Matthews K., et al., 2003, ApJ, 586, L127
Hall D. N. B., Kleinmann S. G., Scoville N. Z., 1982, ApJL, 260, L53
Koyama K., Maeda Y., Sonobe T., Takeshima T., Tanaka Y., Yamauchi S., 1996, PASJ, 48, 249
Leitherer C., 1997, in Luminous Blue Variables: Massive Stars in Transition. Eds: A. Nota & H. Lamers (ASP Conference Series Vol. 120), 58
Levin Y., Beloborodov A. M., 2003, ApJ, 590, L33
Maillard J. P., Paumard T., Stolovy S. R., Rigaut F., 2004, A&A, 423, 155
Melia F., 1992, ApJL, 387, L25
Melia F., 1994, ApJ, 426, 577
Muno M. P., Lu J. R., Baganoff F. K., et al., 2005, submitted to ApJ, astro-ph/0503572
Najarro F., Krabbe A., Genzel R., Lutz D., Kudritzki R. P., Hillier D. J., 1997, A&A, 325, 700
Narayan R., 2002, in Lighthouses of the universe: the most luminous celestial objects and their use for cosmology, ed. M.Gilfanov, R. Sunyaev & E. Churazov (Berlin: Springer), 405
Narayan R., Yi I., 1994, ApJL, 428, L13
Nayakshin S., 2005, A&A, 429, L33
Nayakshin S., Cuadra J., 2005, A&A, 437, 437
Paumard T., Maillard J.-P., Morris M., 2004, A&A, 426, 81
Paumard T., Maillard J. P., Morris M., Rigaut F., 2001, A&A, 366, 466
Porquet D., Grosso N., Belanger G., et al., 2005, A&A, in press, astro-ph/0507283
Proga D., Begelman M. C., 2003a, ApJ, 582, 69
Proga D., Begelman M. C., 2003b, ApJ, 592, 767
Quataert E., 2004, ApJ, 613, 322
Quataert E., Gruzinov A., 2000, ApJ, 539, 809
Reid M. J., Readhead A. C. S., Vermeulen R. C., Treuhaft R. N., 1999, ApJ, 524, 816
Revnivtsev M. G., Churazov E. M., Sazonov S. Y., et al., 2004, A&A, 425, L49
Rockefeller G., Fryer C. L., Melia F., Warren M. S., 2004, ApJ, 604, 662
Ruffert M., Melia F., 1994, A&A, 288, L29
Schödel R., Eckart A., Iserlohe C., Genzel R., Ott T., 2005, ApJL, 625, L111
Schödel R., Ott T., Genzel R., et al., 2002, Nature, 419, 694
Scoville N. Z., Stolovy S. R., Rieke M., Christopher M., Yusef-Zadeh F., 2003, ApJ, 594, 294
Shakura N. I., Sunyaev R. A., 1973, A&A, 24, 337
Springel V., 2005, MNRAS submitted, astro-ph/0505010
Springel V., Di Matteo T., Hernquist L., 2004, MNRAS submitted, astro-ph/0411108
Springel V., Yoshida N., White S. D. M., 2001, New Astronomy, 6, 79
Sunyaev R. A., Markevitch M., Pavlinsky M., 1993, ApJ, 407, 606
Sutherland R. S., Dopita M. A., 1993, ApJS, 88, 253
Wardle M., Yusef-Zadeh F., 1992, Nature, 357, 308
Yuan F., Markoff S., Falcke H., 2002, A&A, 383, 854
Yuan F., Quataert E., Narayan R., 2003, ApJ, 598, 301
Yusef-Zadeh F., Roberts D. A., Biretta J., 1998, ApJL, 499, L159